Available online at www.CivileJournal.org

Civil Engineering Journal

(E-ISSN: 2476-3055; ISSN: 2676-6957)

Vol. 11, No. 06, June, 2025

Stress Concentration Factors in Tubular T-Joint Braces Under Compressive Loads Using Artificial Neural Networks

Adnan Rasul [1*], Saravanan Karuppanan [1], Veeradasan Perumal [1], Mark Ovinis [2], Muhammad Iqbal [3], Saeed Badshah [4], Khurshid Alam [5]

[1] *Department of Mechanical Engineering, Universiti Teknologi PETRONAS, Seri Iskandar 32610, Malaysia.*

[2] *School of Engineering and the Built Environment, Birmingham City University, Birmingham, United Kingdom.*

[3] *Department of Mechanical Engineering, CECOS University of IT & Emerging Sciences, Phase-6 Hayatabad, Peshawar, Pakistan.*

[4] *Department of Mechanical Engineering, International Islamic University, Islamabad 44000, Pakistan.*

[5] *Department of Mechanical and Industrial Engineering, Sultan Qaboos University, Al Khoudh, PC-123, Sultanate of Oman.*

Received 01 February 2025; Revised 06 May 2025; Accepted 11 May 2025; Published 01 June 2025

Abstract

Stress concentration factors (SCFs) are often calculated using formulas based on experimental testing and finite element analysis (FEA). While maximum SCF could occur at any location along the brace axis of the tubular T-joint's brace, only the SCFs at the crown and saddle points can be determined from the available formulae, which can result in imprecise fatigue life determination. The current study presents a methodology to determine the SCFs in T-joints using FEA and ANN. ANNs are more effective than conventional data-fitting techniques at modelling intricate phenomena. In this work, parametric equations to estimate the SCFs of the T-joint's brace under compressive loading were developed. Utilizing parametric equations allows for rapid estimates of SCFs, in contrast to time-consuming FEA and expensive testing. The equations are based on an artificial neural network's training weights and biases (ANN). 625 finite element simulations were performed on tubular T-joints with various dimensions under compressive loads to determine the SCFs at the brace of the T-joint. These SCFs were then used to train an ANN. The weights and biases of the ANN were subsequently used to derive equations for calculating SCFs based on dimensionless parameters. The equations can estimate the SCF of a T-joint brace with less than 7% error and a root mean square error (RMSE) of less than 0.19.

Keywords: Artificial Neural Network; Brace Side SCF; Compressive Loads; Fatigue Design; T-Joint.

1. Introduction

A prevalent form of structural failure in offshore construction is fatigue failure [1], which is frequently caused by cyclic stresses that reoccur [2]. A crucial part of designing offshore structures is figuring out how long each joint will last due to repeated cyclic loads. The fatigue life of each component has a major effect on overall durability and performance. Consequently, precise calculation of the fatigue life for each element is crucial for maintaining the structural integrity and durability of the complete offshore assembly [3].

Generally, these constructions are fabricated using circular hollow section (CHS) tubular members. Aside from CHS, there are various other types of hollow sections, such as Square Hollow Sections (SHS), Rectangular Hollow Sections (RHS), and hybrid sections like CHS-RHS, CHS-SHS, and RHS-SHS [4-8]. CHS are preferred due to their exceptional

* Corresponding author: adnan_22006634@utp.edu.my

http://dx.doi.org/10.28991/CEJ-2025-011-06-013

bending strength, resistance to buckling in any direction, high strength-to-weight ratio, and minimal wave resistance [9]. The tubular joint comprises branching elements, referred to as braces, and the main structural element, chord [3]. The T-joint configuration with a brace perpendicular to the chord is shown in Figure 1.

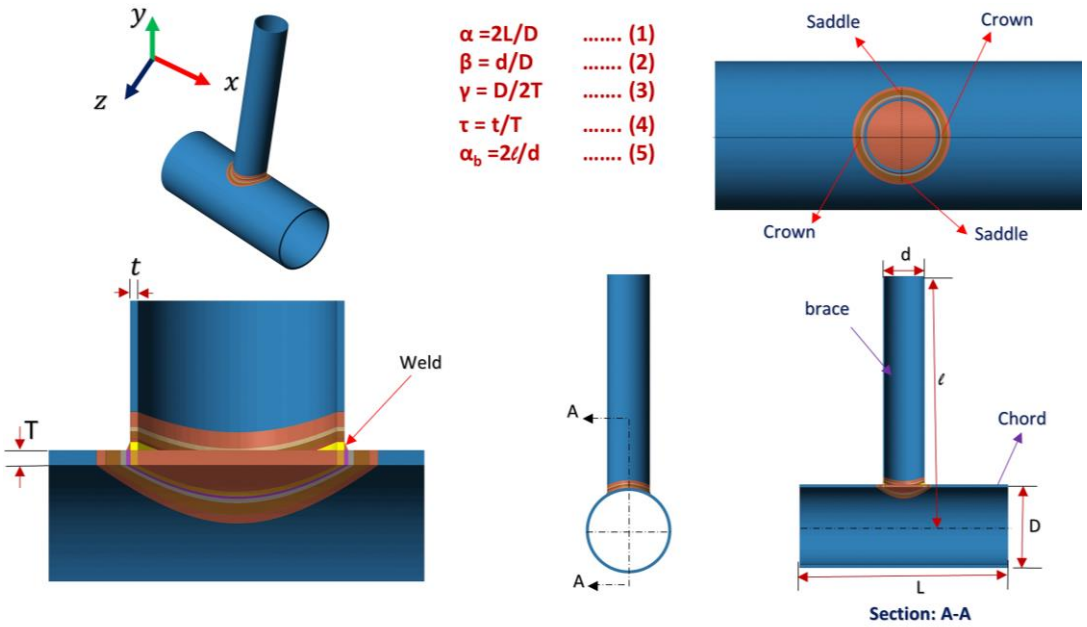

Figure 1. T joint configuration

S-N curves from design codes are used to compute the number of cycles (N) before fatigue failure once the maximum stress or hotspot stress (HSS) is known [10-15]. The HSS requires precise SCF calculations. Accurately predicting the number of cycles before the fatigue failure ensures the long-lasting durability and reliability of these structures. The calculation of SCFs involves complex relationships due to their dependence on various factors, such as the shape of the joint, the magnitude of the applied stress, the size and type of the weld, and the distance from the weld. ANNs can be used to develop parametric equations to account for the non-linear relationship of these factors, leveraging large datasets for enhanced accuracy. Despite five decades of intensive research, the design codes' accessible equations address the SCF equations only at two points: the saddle and the crown [16-22]. This may lead to incorrect calculations of fatigue cycles due to the potential occurrence of hotspot stress between these two sites [23].

The multidirectional attributes of the sea impose multiaxial stresses on offshore structures, resulting in the presence of HSS at locations other than the saddle and crown [24]. Gulati et al. [25] advocated for the calculation of HSS by integrating stresses from all axes. This methodology is deemed accurate and comprehensive [24] by the UEG [21] and the API [26].

The fatigue life is typically assessed using experimentation and finite element analysis. The numerical model is normally validated experimentally, which is expensive. FEA is utilized for additional analysis and to derive numerical equations. These equations provide the SCF values, which, along with nominal brace load, are used to calculate the HSS and, eventually, the fatigue life through the design codes' S-N curve. In the past 35 years, several parametric models have been developed to determine SCFs for tubular joints [16–22]. The Lloyd's Register (LR) [18] extensively assessed mathematical equations for offshore connections developed in the past five decades [16–22]. The equations were derived through an empirical investigation of tubular joints. The LR equations [18] minimize the difference between the actual and estimated SCF for two positions only (saddle & crown).

Efthymiou [22] presented SCF equations for two positions only (saddle and crown) for KT, X, T, Y, and K joints that are presently employed in the API [26], DNV [27] and ISO-19902 [28]. However, they result in frequent underpredictions, as they are based on mean fitness [18]. The equations by Wordsworth/Smedley (W/S) from the acrylic material tubular joints without fillet weld address the SCF for the same two positions only [18]. The UEG equations [21] were derived from the W/S and Wordsworth equations by incorporating an adjustment to account for joints characterized by β (>0.6) and high γ (>20) values. These equations [21] were produced through least squares curve fitting, resulting in conservative SCFs [18]. Additionally, Vinas-Pich [24] found that the stress distribution equations of the UEG [21] are not accurate enough for the entire brace-chord junction.

Kaung et al. [19] formulated equations to calculate the SCFs of KT, K, T, and Y joints using a finite element model. The equations were formulated based on statistical analysis of data obtained from examining FE joints. Precise

localization of the stress hotspot surrounding the weld is not possible; instead, it is classified as either chord-side or brace-side. The SCFs are likely to be underestimated for extended chord lengths, as Kuang generally employed joints with shorter chord lengths. [18]. Smedley and Fisher [16] developed equations for joints (T, X, Y, KT, and K), although the equations are not applicable for calculating the SCF around the intersection.

While stress distribution along the weld line of the tubular joint is important [29-33], most research has concentrated on finding the SCF at the saddle and crown locations. In this work, the SCF of a T-joint's brace under compressive load is modeled using Artificial Neural Networks (ANNs). ANNs are a successful tool for approximating complex phenomena, as demonstrated in previous studies [34, 35], and can generate comprehensive and precise predictions [23, 29, 36, 37]. It offers several advantages, such as its capacity to accurately approximate universal functions, perform parallel data processing, and successfully manage nonlinearity [29, 36]. The calculation of SCFs involves complex non-linear relationships due to their dependence on various factors, such as the shape of the joint, the magnitude of the applied stress, the size and type of the weld, and the distance from the weld. Parallel processing with ANNs can expedite this process, while their ability to learn from large datasets enhances accuracy and is particularly well-suited for these requirements.

2. Research Methodology

The Design of Experiment (DoE) dataset was simulated using ANSYS [38]. The results from the DoE were subsequently transferred to MATLAB [39]. The nntool program of MATLAB was employed to construct a neural network model. The parameters were taken as input, while the SCF was the output. The model was trained in nntool, and weights and biases were used to derive mathematical formulas for SCFs.

For ANN-based mathematical modelling, the first step is to determine the input parameters range. Following this step, design combinations are established, and then, FEA is performed. In the end, the equations are constructed by the outputs of the ANN. The methodology of this concept is depicted in Figure 2. The DOE was generated using a range of design factors frequently employed in offshore structures and modelled using Finite Element Analysis (FEA). The results were imported into MATLAB [39] to construct a neural network model. The equations were later formulated using the weights and biases from the ANN as acquired through MATLAB [39]. These stages are explained in depth in the following subsections.

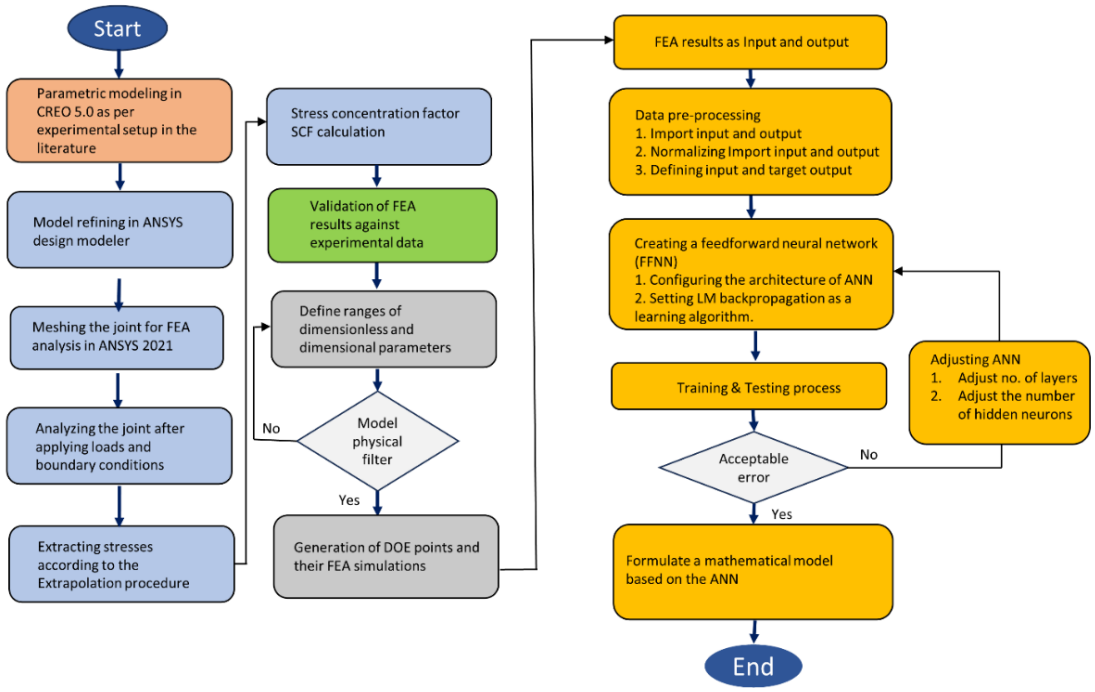

Figure 2. Flow diagram for ANN-based SCF modelling

2.1. Finite Element Modelling

Incorporating both dimensionless and dimensional parameters, finite element modelling of T-joints was conducted using ANSYS 2021 [38] and CREO 5.0 [40]. The models were built based on DOE in CREO [40] and further improved in ANSYS [38]. ANSYS 2021R1 software was utilized to determine stress concentration factors in tubular joints through linear elastic static analysis [41, 42].

2.2. Parametric Modelling

The tubular T-joint was modelled utilizing CREO 5.0 [40]. The T-joint models (Figure 1) were developed through parametric equations, integrating parameters as variables. The parametric modelling accelerated the regeneration process for the subsequent iteration.

$$\alpha = 2L/D \quad (1)$$

$$\beta = d/D \quad (2)$$

$$\gamma = D/2T \quad (3)$$

$$\tau = t/T \quad (4)$$

$$\alpha_b = 2l/d \quad (5)$$

where L, D, and T are the length, diameter, and thickness of the chord, respectively, and t, l and d are the thickness, length and diameter of the brace, respectively (Figure 1).

Parametric modelling allowed for the rapid and effective modification of the model based on the DoE. The creation of sub-zone meshing, as illustrated in Figure 3, was achieved through sub-components-based modelling.

2.3. Weld Profile

A proper evaluation of the Stress Concentration Factor (SCF) requires an accurate weld profile. AWS D 1.1 standard [43] was followed for weld dimensions. The weld profile adhered to full joint penetration (CJP) weld profiles [44] outlined by AWS D 1.1 and discussed in detail by Lotfollahi-Yaghin et al. [31]. Residual stresses are minimized through post-heating after fabrication, which helps reduce welding-induced stresses in tubular joints [45].

2.4. Material Model

The characteristics of the steel material for the T-joint were derived from the experimental test results conducted by Masilamani & Nallayarasu [46] and are presented: Yield stress300 MPa; Ultimate stress 415 MPa; Young's modulus 207.9 GPa; Poisson's ratio 0.29.

2.5. Meshing

A finer mesh size was utilized for areas of high concentration, whereas a coarser mesh size was employed for areas of lower concentration. The sub-components were individually meshed (refer to Figure 3), and rigid contacts in ANSYS [38] were utilized to establish their connection.

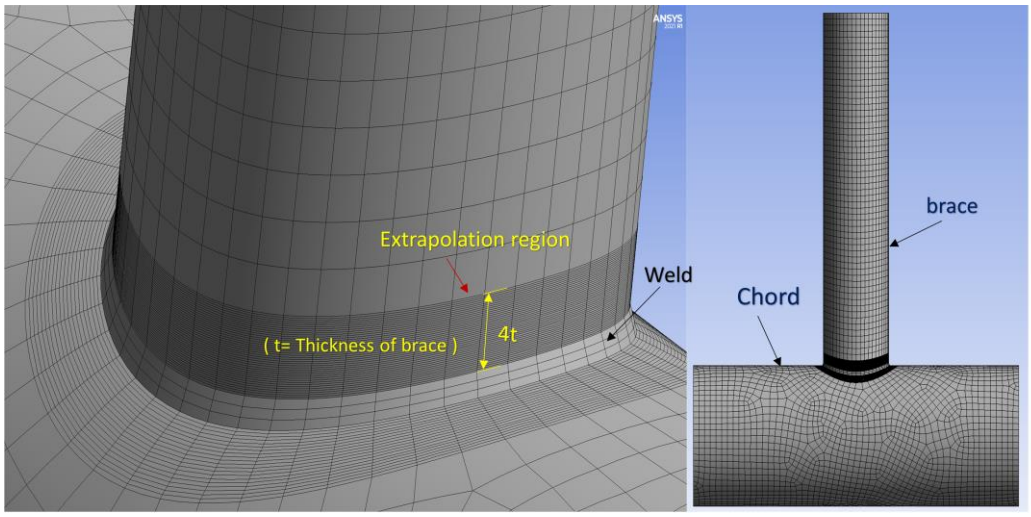

Figure 3. Mesh created in ANSYS 2021 for a T-joint's FEA analysis [38]

A mesh sensitivity study was initially conducted to evaluate the accuracy and efficiency of the FE model, offering direction for the optimized mesh before finalizing the FEA models.

2.6. Boundary Conditions and Loads

The load magnitudes were chosen such that the deformation is within the linear elastic region [47]. The chord's end faces were fixed, and a 10 MPa stress was exerted at the top face of the brace. Keeping the stresses in the DoE's weakest joint below the elastic limit was the deciding factor in selecting this stress. Figure 4 displays the boundary conditions and applied axial load.

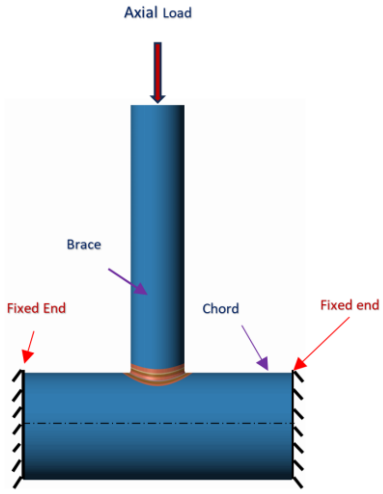

Figure 4. Boundary conditions and axial load

2.7. SCF Calculation

To automate stress determination and extrapolation, a Python code was incorporated into ANSYS. This code retrieves the stress and positional coordinates of the reference locations and calculates the stress at the weld toe by linear extrapolation. The Python script measures the von Mises stresses at 0.4*t and 1.4*t from the weld toe (where t is the thickness of the brace) and then extrapolate it. The extrapolation region was partitioned into 48 equidistant segments from 0° to 360°. This division allows for stress measurements at a 15° angle relative to the axis of the brace. Twenty-four sites were chosen to assess stress around the brace axis, as illustrated in Figure 5.

$$SCF = {\sigma_{hotspot\ stress}}/{\sigma_{nominal\ stress}} \quad (6)$$

The extrapolation points and the extrapolation procedure, as shown in Figure 5, followed the guidelines of IIW-XV-E-(1999) [48].

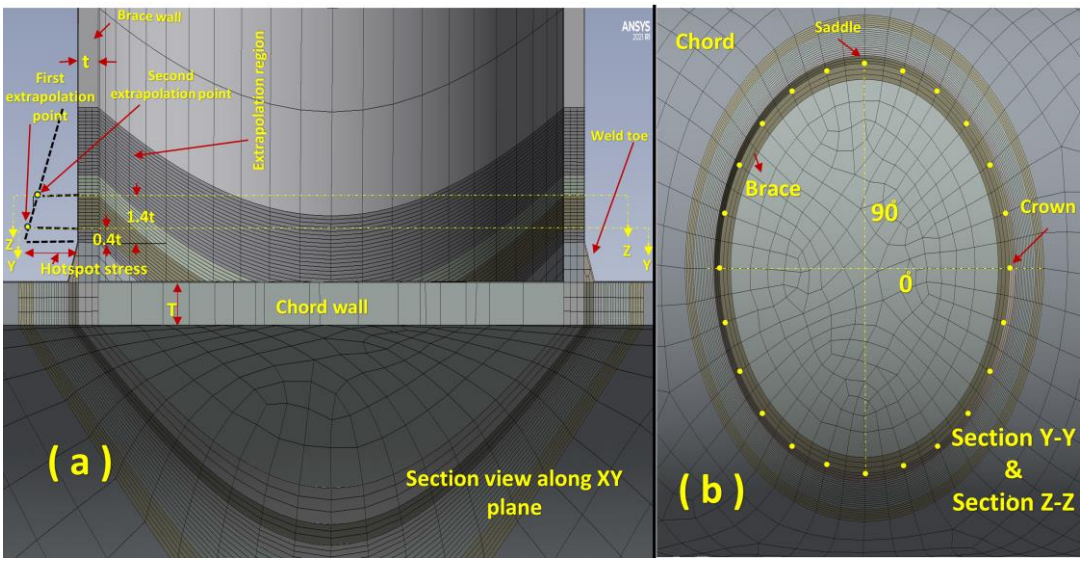

Figure 5. Extrapolation points and the linear extrapolation [48]

The length of the brace has no impact on the SCF, given that the ratio α_b (where $\alpha_b = 2\ l/d$) is above a crucial threshold (Chang et al. [24]). So, to exclude it from the parametric study, the brace length was set to 1000mm for the DOE.

2.8. Design Parameters and Their Ranges

The parametric equations to build the model employ the design variables as a mathematical function. Typical ranges of dimensionless parameters usually employed in offshore structures were selected for design variables.

2.9. Design's Dataset for DoE

Two phases were involved in the development of the DoE design dataset. Firstly, all possible combinations were made for the parameter's entire ranges. Due to the enormous number of possible combinations, a partial factorial design was utilized to restrict the number of simulations that were performed, with five distinct values assigned to each parameter. For each variable, e.g., α, all possible combinations were made with five different values of other variables (β,γ and τ). The partial factorial design resulted in 625 design points, which were simulated for DoE. The entire range of variables was modelled in Creo 5.0 [40] for physical filtering to ensure that none of them created an error in the regeneration of the T-joint. The parametric modelling facilitated rapid and efficient model regeneration.

2.10. MATLAB *nntool* for ANN Modelling

The MATLAB nntool was used for modelling with artificial neural networks (ANN), which are based on the universal approximation theorem. According to this theorem, a neural network provided with certain inputs is capable of approximating continuous functions [49]. To determine the brace's Stress Concentration Factor (SCF) under compressive loads, this research combined ANN and FEA to build empirical equations. The dimensionless parameters and the SCFs were the input and output data for MATLAB [39], respectively. These datasets were then imported into the nntool package in MATLAB to generate a neural network. Due to its efficient second-order convergence rate [29, 36, 49-51], the Levenberg–Marquardt backpropagation method was employed for supervised learning. Figure 6 illustrates the design of a typical neural network. Two inputs, three neurones, and two outputs are represented in the input, hidden, and output layers, respectively.

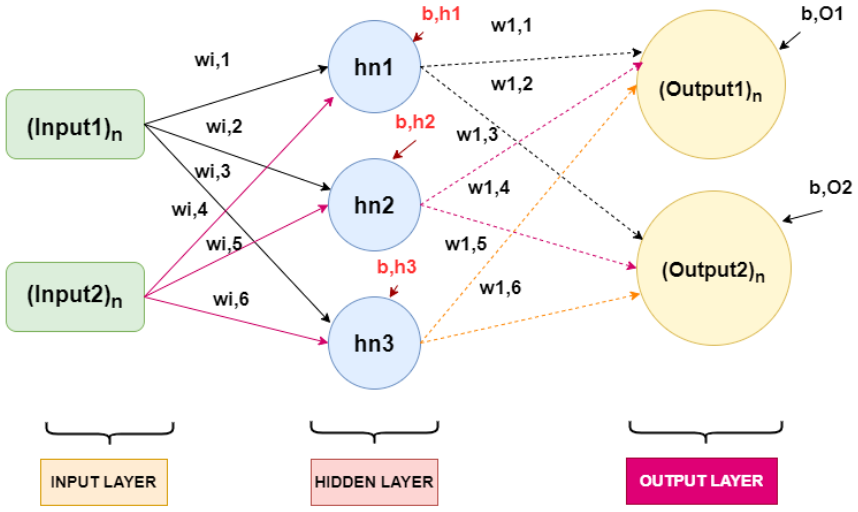

Figure 6. Typical ANN model

The designated input and output data were used to train the ANN. Equation 7 is used in the hidden layers, and Equation 8 is the linear transfer function in the input and output layers. To evaluate the ANN's ability to generate outcomes that were very consistent with the training data, the R^2 value of the model was utilized. The R^2 value ranges from 0.0 to 1.0 and indicates the correlation between the training data points and the ANN plot's regression line. Correlation is considered strong when the R^2 value is high.

$$a(x) = \frac{2}{(1+e^{-2x})-1} \quad (7)$$

$$f(x) = x \quad (8)$$

2.11. Formulation of Mathematical Model

The ANN's biases and weights were used to obtain the equations. An ANN is represented by a matrix in Equations 9 and 10. Neurons in the next hidden layer ($h\,nx$) are linked to the inputs (ipx) by weights (WWx). An activation function A(x) is applied after multiplying the values by their respective weights and adding them together. A hidden layer neuron receives input from the cumulative total up to the output layer, and the output is then mixed with a bias

value (Bx).

$$\begin{bmatrix} hn1 \\ hn2 \end{bmatrix} = \begin{bmatrix} W1 & W3 & W5 \\ W2 & W4 & W6 \end{bmatrix} \begin{bmatrix} ip1 \\ ip2 \\ ip3 \end{bmatrix} + \begin{bmatrix} B1 \\ B2 \end{bmatrix} \quad (9)$$

$$[op] = [W7 \quad W8] \begin{bmatrix} hn1 \\ hn2 \end{bmatrix} + [B3] \quad (10)$$

3. Results

3.1. Establishment of the Precise Ranges of Design Parameters

The geometry of the T-joint is defined by parameters (Figure 1). To build a DoE that meets the standards for offshore structures, these parameters and their ranges were chosen [18, 52]. The variable ranges are presented in Table 1. The simulation dataset included 625 design points.

Table 1. Parameters and their corresponding ranges

Sr.No.	Type of parameter	Parameter	Range	References
1	Dimensionless	α	8-40	[18, 52]
2		β	0.3-0.7	
3		γ	12-28	
4		τ	0.4-1	
5	Dimensional	Θ	90˚	
6		D	300mm	
7		l	1000mm	

Table 2 presents the results of the sensitivity analysis. The experimental and FEA results were compared for sensitivity analysis. A mesh of 16757 elements was used after the sensitivity analysis.

Table 2. Mesh sensitivity analysis

Serial No.	Mesh elements	SCF_{crown} (FEA)	SCF_{saddle} (FEA)	SCF_{crown} FEA/ SCF_{crown} (Exp)	SCF_{saddle} FEA/ SCF_{saddle} (Exp)
1	14309	1.68	4.16	0.93	0.85
2	16757	1.83	4.54	1.02	0.93
3	18777	1.83	4.54	1.02	0.93

The FEA model was validated using HSE OTH 354 experimental results for the T-joint UKOSRP II T215 [18]. The joint's geometric parameters were the same as those of the experimental test model (Table 3).

Table 3. Chord diameter and the other geometrical parameters used for the validation

Reference joint	D (mm)	α	β	γ	τ
UKOSRP II joint T215 [18]	914	5	0.5	14.3	0.5

For validation purposes, Table 4 compares the FEA results with the experimental test results [18], the American Petroleum Institute (API) [26], and the LR equations [18]. Table 4 presents the percentage error among the experimental test results and those derived from the LR equations [18], API equations [34], and the current FEA study, respectively. The present study had a maximum error of 7.93%, suggesting that the FE model can accurately predict the SCF.

Table 4. Comparison of LR equations [18], API [26], and experimental test results [18] with FEA results

Joint	Position	Exp. results	LR	API	FEA results	% Err. 1	% Err. 2	% Err. 3
UKOSRP II joint T215	Crown	1.80	1.89	2.24	1.83	-4.90	-19.71	-1.64
	Saddle	4.90	4.53	5.44	4.54	8.26	-9.99	7.93

3.2. Creation of the Design's Dataset

ANSYS [38] was used to run the simulations after the FE model was verified. The stress values were acquired using a Python script at a 15° angle around the axis of the brace in ANSYS Mechanical [38] and subsequently stored. Additionally, the von Mises stresses were calculated at 0.4*t and 1.4*t. Hotspot stresses at the weld toe were extrapolated

based on the calculated stresses. Due to the fact that linear extrapolation and non-linear extrapolation exhibit less than 10% variation, the linear method was implemented [18]. Von Mises stresses in the T-joint around the weld line are shown in Figure 7. The areas near the weld line are under higher stresses as compared to the areas away from the weld line. The International Institute of Welding's IIW-XV-E-(1999) [48] guidelines were followed when estimating hotspot stress at the weld toe. Equation 6 was used to calculate SCFs from these hotspot stress values, which were then employed to train the ANN. In total, 625 design combinations were used to generate outputs, resulting in 24 SCFs at 15° intervals per cycle.

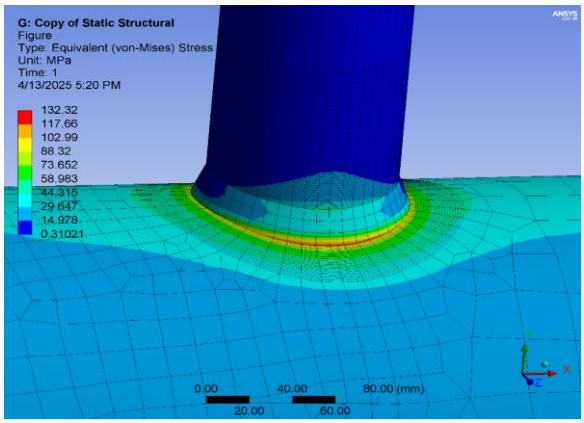

Figure 7. Von mises stresses in T-joint

3.3. Using MATLAB's nntool for ANN modelling

The dataset used for training consisted of 625 simulated design points. The ANN model generated SCF values at 15° intervals using input parameters (α, β, γ, τ). A feed-forward neural network (FFNN) with input, output, and one or more hidden layers was selected. The training dataset comprised 70%, while testing and validation received 15% each [37].

The architecture of the developed ANN models is shown in Figure 8. The optimal architecture of the neural network was determined by trial and error by adjusting the total number of hidden layers and neurons [34]. A neural network with a single hidden layer comprising nine neurons was used.

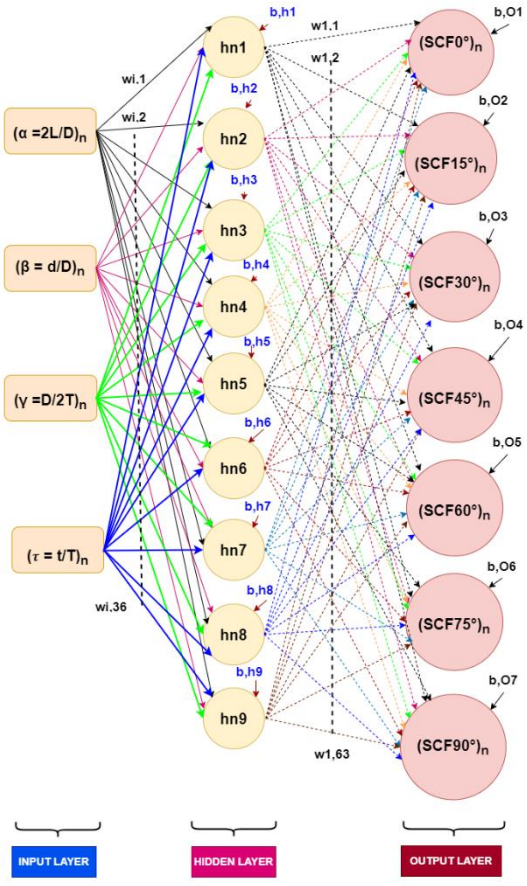

Figure 8. The developed ANN

Figure 9 displays regression plots for the ANN created using MATLAB R2021 [39]. The diagrams include separate plots for training, validation, and testing and a combined view of all three. The linear regression line of best fit between the intended output and the output of the ANN is illustrated in these plots. The solid line represents the true line of the strongest fit, whereas the dashed line represents the ideal or perfect outcome. In each plot, the solid and dotted lines align closely, as observed in Figure 9, showing that the ANN's outputs are very consistent with the data used for training. The ANN achieved an R^2 value of 0.99916 (Figure 9), demonstrating exceptional accuracy. The R^2 value of 0.99916 demonstrates a robust correlation between the SCF predictions generated by the ANN and those obtained from the FEA analysis.

Figure 9 shows trained ANN validation. Empirical modelling utilized the weights for each neuron and the biases for each layer.

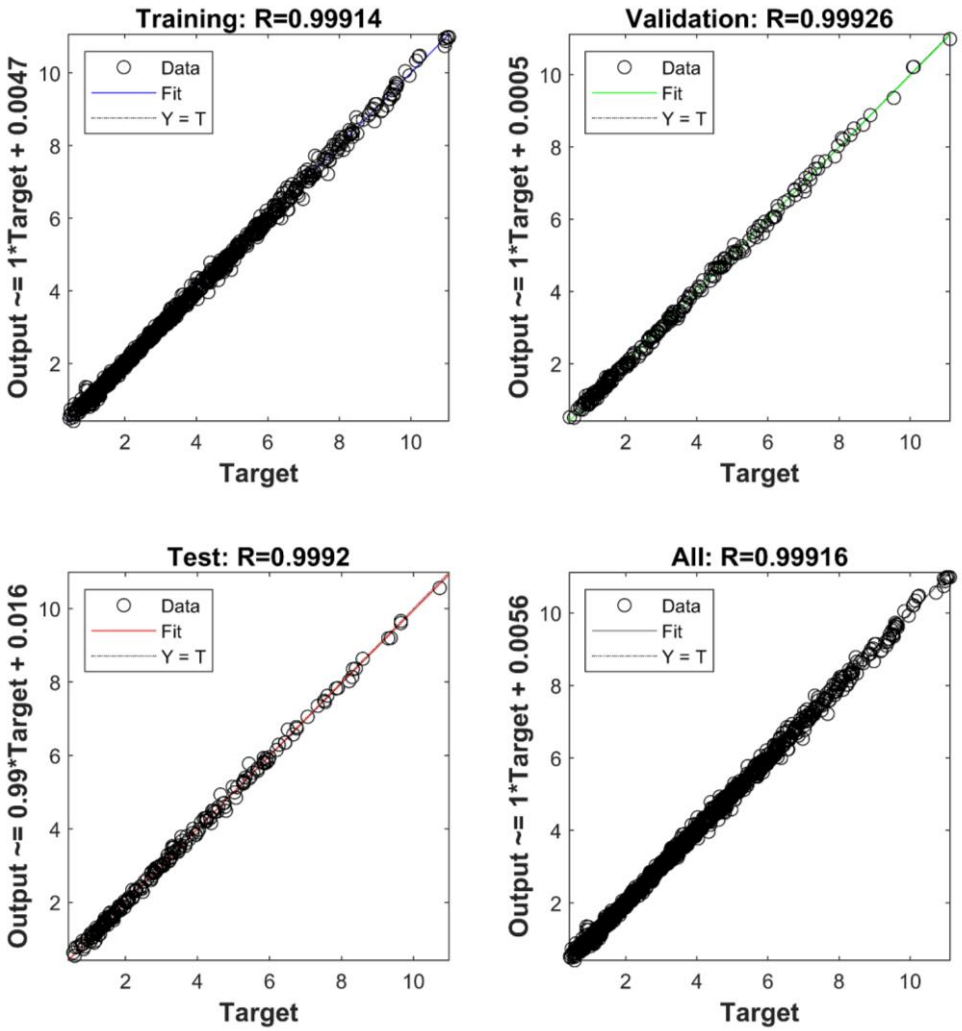

Figure 9. Trained ANN regression plot

3.4. Development of an Empirical Model

The development of an empirical model involved exporting a matrix containing the ANN's weights and biases. In order to avoid particular variables being very dominant, the inputs were normalized, while the outputs were denormalized. Equations 11 and 12 were employed for normalization and denormalization, respectively. For SCFs, empirical formulas are provided by equations 13 and 14.

$$i_{normalized} = i_{n,min} + \frac{(i_{n,max} - i_{n,min})(i - i_{min})}{(i_{max} - i_{min})} \quad (11)$$

$$o_{denormalized} = o_{min} + \frac{(o_n - o_{n,min})(o_{max} - o_{min})}{(o_{n,max} - o_{n,min})} \quad (12)$$

where $i_{n,max}$ = 1, where i_{max} is the maximum of the initial input data. $i_{n,min}$ = -1, where i_{min} is the minimum of the initial input data. $o_{n,max}$ = 1, where o_{max} = maximum value derived from the SCF data utilized in the training process. $o_{n,min}$ = -1, where o_{min} = minimum value derived from the SCF data utilized in the training process.

$$\begin{bmatrix} h1 \\ h2 \\ h3 \\ h4 \\ h5 \\ h6 \\ h7 \\ h8 \\ h9 \end{bmatrix} = \begin{bmatrix} -0.770 & -8.445 & -0.870 & -1.192 \\ 0.313 & -1.045 & 0.234 & -0.115 \\ -0.344 & -1.435 & 1.579 & -9.740 \\ -0.220 & 0.497 & 0.441 & -0.184 \\ -0.167 & 0.229 & 0.233 & -0.187 \\ -0.040 & 0.442 & 0.042 & -2.153 \\ 5.383 & -0.214 & -0.607 & -0.330 \\ -0.028 & 0.326 & 0.154 & -1.786 \\ -0.436 & -3.791 & 0.127 & 0.341 \end{bmatrix} \begin{bmatrix} \alpha_n \\ \beta_n \\ \gamma_n \\ \tau_n \end{bmatrix} + \begin{bmatrix} 7.886 \\ 0.185 \\ -6.755 \\ 1.075 \\ 0.773 \\ 1.340 \\ 6.279 \\ 1.037 \\ -3.506 \end{bmatrix} \quad (13)$$

$$\begin{bmatrix} SCF\ 0^{\circ} \\ SCF\ 15^{\circ} \\ SCF\ 30^{\circ} \\ SCF\ 45^{\circ} \\ SCF\ 60^{\circ} \\ SCF\ 75^{\circ} \\ SCF\ 90^{\circ} \end{bmatrix} = \begin{bmatrix} -0.093 & -0.751 & 0.403 & 4.287 & -8.398 & -1.374 & -0.710 & 2.171 & 0.648 \\ -0.171 & -0.510 & 0.368 & 4.239 & -7.924 & -0.710 & -0.620 & 1.483 & 0.426 \\ -0.244 & -0.071 & 0.218 & 5.182 & -8.083 & 0.272 & -0.453 & 0.471 & 0.137 \\ -0.218 & 0.730 & -0.177 & 4.393 & -4.996 & -0.706 & 0.094 & 1.109 & -0.117 \\ -0.227 & 0.904 & -0.380 & 1.953 & -0.688 & -1.478 & 0.431 & 1.530 & -0.332 \\ -0.306 & 0.948 & -0.450 & 0.352 & 1.810 & -1.828 & -0.550 & 1.722 & -0.471 \\ -0.339 & 0.942 & -0.476 & -0.170 & 2.614 & -2.067 & 0.601 & 1.926 & -0.511 \end{bmatrix} \begin{bmatrix} h1 \\ h2 \\ h3 \\ h4 \\ h5 \\ h6 \\ h7 \\ h8 \\ h9 \end{bmatrix} + \begin{bmatrix} 3.129 \\ 2.580 \\ 1.600 \\ -0.269 \\ -1.666 \\ -2.241 \\ -2.446 \end{bmatrix} \quad (14)$$

The empirical model was validated against an independent dataset that differed from the testing, training, and validation datasets. With their respective maximum absolute differences, percentage errors, and root-mean-squared errors (RMSEs), Table 5 details five verification design points, which were distinct from training, validation and testing datasets. The comparison of SCF from the proposed ANN model and the SCF from FEA in ANSYS Workbench [38] is shown in Figures 10 and 11.

Table 5. Empirical model's verification results

Sr. No.	α	β	γ	τ	Max. absolute difference	Maximum % Error	RMSE (Route mean square error)
1	39.80	0.69	12.30	0.71	0.34	-6.55	0.18
2	23.90	0.52	12.15	0.99	0.20	4.42	0.09
3	31.75	0.31	19.90	0.41	0.14	-5.35	0.09
4	32.10	0.49	20.12	0.42	0.26	-4.06	0.13
5	31.90	0.32	24.13	0.73	0.39	-6.53	0.19

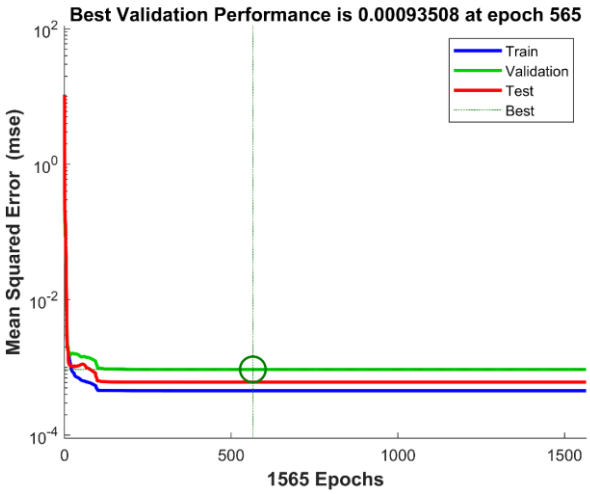

Figure 10. Trained ANN validation

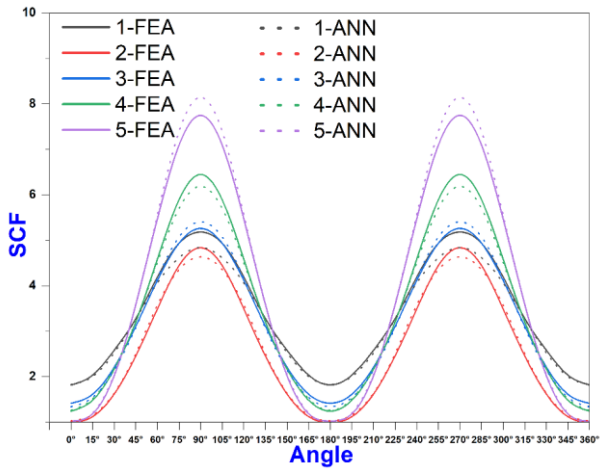

Figure 11. Comparative Analysis of FEA and ANN Outcomes

The resulting equations yield a highly accurate SCF calculation, with an error of less than 7% and an RMSE of under 0.2 in comparison to the SCF derived via FEA. ANN models learn from training data to predict outcomes within a ±7% margin of error for new, unseen values. Variability in predictions stems from the model's complexity in capturing non-linear relationships. Under compressive loads, these formulae can be used to swiftly calculate the SCF of the T-joint's brace.

4. Conclusion

The equations derived using ANN can accurately calculate the SCFs of a tubular T-joint's brace subjected to compressive loads. The combination of FEA and ANN is an effective approach to developing equations for calculating SCFs. These equations can accurately determine the SCFs of a T-joint's brace under compressive load, exhibiting an error rate below 7% and a root mean square error (RMSE) under 0.2. These equations precisely compute the SCF at a 15° offset from the crown to the saddle position. Practicing engineers can employ equations 13 and 14 to accurately and efficiently determine hotspot stress to mitigate the risks concerning offshore structure fatigue failure. This research contributes to the safety and reliability of offshore structures by enabling more precise assessments of stress distribution. The same method can be applied to calculate the SCF for the inclined braces of the tubular joint. Furthermore, this methodology can be used for various types of connections subjected to diverse loading situations to formulate equations enabling effective SCF computations.

5. Nomenclature

D	Chord diameter	d	Brace diameter
T	Chord thickness	t	Brace thickness
θ	Angle between the brace and the chord	L	Chord length
ℓ	Brace length	β	Ratio of the diameter of brace and chord
γ	Ratio of chord's diameter and twice chord's thickness	τ	Ratio of brace thickness to chord thickness
α	Ratio of twice the length of the chord to the diameter of the chord	α_b	Ratio of twice the length of brace to the diameter of the brace
r	Brace radius	t	Brace thickness
SCF	Stress Concentration Factors	ANN	Artificial Neural Network
FEA	Finite Element Analysis	DOE	Design of Experiments
R^2	Coefficient of determination	IPB	In-Plane Bending Loads
OPB	Out-of-Plane Bending Loads	i_{max}	Maximum of original input data
i_{min}	Minimum of original input data	o_{max}	Maximum of SCF data used for training
o_{min}	Minimum of SCF data used for training	F	Force applied on the top of the brace
AWS	The American welding society	IIW	International Institute of Welding
API	American Petroleum Institute	DNN	Deep Learning Neural Network
GA	Genetic Algorithm	GBDT	Gradient Boosting Decision Trees
$\sigma_{nominal\ stress}$	Nominal brace stress applied on brace	$\sigma_{hotspot\ stress}$	Maximum stress along the weld toe
FFNN	Feed-Forward Neural Network Design	DNV	Det Norske Veritas
UEG	Underwater Engineering Group	HSS	Hotspot stress
CHS	Circular Hollow Sections	RHS	Rectangular hollow sections
SHS	Square Hollow Sections	N	Fatigue load cycles
σ_1 , σ_2	Stresses at Extrapolation points	Bx	Bias value
A(x)	Activation function	$h\,nx$	Neurons in the hidden layer
ipx	Input parameters	WWx	ANN weights

6. Declarations

6.1. Author Contributions

Conceptualization, A.R. and S.K.; methodology, A.R. and M.I.; software, A.R. and K.A.; validation, A.R. and V.P.; writing—original draft preparation, A.R. and M.I.; writing—review and editing, A.R., S.K., and M.O.; visualization, A.R. and V.P.; supervision, S.K.; project administration, S.K. and V.P.; funding acquisition, S.K. All authors have read and agreed to the published version of the manuscript.

6.2. Data Availability Statement

The data presented in this study are available on request from the corresponding author.

6.3. Funding

This research received funding from Yayasan Universiti Teknologi PETRONAS under grant No. 015LC0-443.

6.4. Conflicts of Interest

The authors declare no conflict of interest.

7. References

[1] Ma, M., Liu, X., Yu, X., & Wang, X. (2023). Fatigue life prediction for notched specimen considering modified critical plane method. Fatigue and Fracture of Engineering Materials and Structures, 46(3), 1031–1044. doi:10.1111/ffe.13917.

[2] Liu, X., & Ma, M. (2023). Cumulative fatigue damage theories for metals: review and prospects. International Journal of Structural Integrity, 14(5), 629–662. doi:10.1108/IJSI-09-2022-0119.

[3] Rasul, A., Karuppanan, S., Perumal, V., Ovinis, M., & Iqbal, M. (2024). Ultimate Strength of Internal Ring-Reinforced KT Joints Under Brace Axial Compression. Civil Engineering Journal (Iran), 10(5), 1543–1560. doi:10.28991/CEJ-2024-010-05-012.

[4] Chandramohan, D. L., Roy, K., Taheri, H., Karpenko, M., Fang, Z., & Lim, J. B. P. (2022). A State-of-the-Art Review of Fillet Welded Joints. Materials, 15(24). doi:10.3390/ma15248743.

[5] Feng, R., Tang, C., Roy, K., Chen, Z., Chen, B., & Lim, J. B. P. (2020). An experimental study on stress concentration factors of stainless steel hybrid tubular K-joints. Thin-Walled Structures, 157, 107064. doi:10.1016/j.tws.2020.107064.

[6] Feng, R., Chen, L., Chen, Z., Chen, B., Roy, K., & Lim, J. B. P. (2021). Experiments on stainless steel hybrid K-joints with square braces and circular chord. Journal of Constructional Steel Research, 185, 106865. doi:10.1016/j.jcsr.2021.106865.

[7] Feng, R., Tang, C., Chen, Z., Roy, K., Chen, B., & Lim, J. B. P. (2021). A numerical study and proposed design rules for stress concentration factors of stainless steel hybrid tubular K-joints. Engineering Structures, 233, 111916. doi:10.1016/j.engstruct.2021.111916.

[8] Feng, R., Xu, J., Chen, Z., Roy, K., Chen, B., & Lim, J. B. P. (2021). Numerical investigation and design rules for stress concentration factors of stainless-steel hybrid tubular joints. Thin-Walled Structures, 163, 107783. doi:10.1016/j.tws.2021.107783.

[9] Saini, D. S., Karmakar, D., & Ray-Chaudhuri, S. (2016). A review of stress concentration factors in tubular and non-tubular joints for design of offshore installations. Journal of Ocean Engineering and Science, 1(3), 186–202. doi:10.1016/j.joes.2016.06.006.

[10] Xu, X., Shao, Y., Gao, X., & Mohamed, H. S. (2022). Stress concentration factor (SCF) of CHS gap TT-joints reinforced with CFRP. Ocean Engineering, 247, 110722. doi:10.1016/j.oceaneng.2022.110722.

[11] Petinov, S., & Guchinsky, R. (2018). Criteria for Fatigue Failure of Materials: Application in Fatigue Assessment of Structures. Advanced Engineering Forum, 26, 1–8. doi:10.4028/www.scientific.net/aef.26.1.

[12] Wardenier, J., Kurobane, Y., Packer, J. A., Van der Vegte, G. J., & Zhao, X. L. (2008). Design guide for circular hollow section (CHS) joints under predominantly static loading. Construction with hollow steel sections, CIDECT, Geneva, Switzerland.

[13] Nassiraei, H., & Rezadoost, P. (2020). Stress concentration factors in tubular T/Y-joints strengthened with FRP subjected to compressive load in offshore structures. International Journal of Fatigue, 140, 105719. doi:10.1016/j.ijfatigue.2020.105719.

[14] Lai, J., Wang, Y., Wei, Y., Liang, J., & Liu, X. (2022). The prediction of residual life of liquid-storage tank considering the tank wall surface state. International Journal of Structural Integrity, 13(6), 985–998. doi:10.1108/IJSI-05-2022-0070.

[15] Iqbal, M., Karuppanan, S., Perumal, V., Ovinis, M., Iqbal, M., & Rasul, A. (2024). Optimization of fibre orientation for composite reinforcement of circular hollow section KT-joints. International Journal of Structural Integrity, 15(4), 717–730. doi:10.1108/ijsi-04-2024-0054.

[16] Smedley, P., & Fisher, P. (1991). Stress concentration factors for simple tubular joints. ISOPE International Ocean and Polar Engineering Conference, 11-16 August, 1991, Edinburgh, United Kingdom.

[17] Hellier, A. K., Connolly, M. P., & Dover, W. D. (1990). Stress concentration factors for tubular Y- and T-joints. International Journal of Fatigue, 12(1), 13–23. doi:10.1016/0142-1123(90)90338-F.

[18] OTH-354 (1997). Stress Concentration Factors for Simple Tubular Joints: Assessment of Existing and Development of New Parametric Formulae. UK Health and Safety Executive, Bootle, United Kingdom.

[19] Kuang, J. G., Potvin, A. B., & Leick, R. D. (1975). Stress Concentration in Tubular Joints. Offshore Technology Conference. doi:10.4043/2205-ms.

[20] Wordsworth, A. C., & Smedley, G. P. (1978). Stress concentrations at unstiffened tubular joints. European Offshore Steels Research Seminar, 27-29 November, 1978, Abington Hall, United Kingdom.

[21] UEG. (1985). Design of tubular joints for offshore structures. United European Gastroenterology (UEG), Vienna, Austria.

[22] Efthymiou, M. (1988). Development of SCF formulae and generalised influence functions for use in fatigue analysis. OTJ 88, Surrey, United Kingdom.

[23] Iqbal, M., Karuppanan, S., Perumal, V., Ovinis, M., & Nouman, H. (2023). Empirical modeling of stress concentration factors using finite element analysis and artificial neural networks for the fatigue design of tubular KT-joints under combined loading. Fatigue & Fracture of Engineering Materials & Structures, 46(11), 4333–4349. doi:10.1111/ffe.14122.

[24] Chang, E., & Dover, W. D. (1999). Parametric equations to predict stress distributions along the intersection of tubular X and DT-joints. International Journal of Fatigue, 21(6), 619–635. doi:10.1016/S0142-1123(99)00018-3.

[25] Gulati, K. C., Wang, W. J., & Kan, D. K. Y. (1982). An Analytical Study of Stress Concentration Effects in Multibrace Joints Under Combined Loading. Offshore Technology Conference. doi:10.4043/4407-ms.

[26] API Recommended Practice 2A-WSD. (2007). Recommended Practice for Planning, Designing and Constructing Fixed Offshore Platforms — Working Stress Design. American Petroleum Institute (API), Washington, United States.

[27] DNVGL-RP-C203. (2024). Fatigue design of offshore steel structures. DNV GL, Bærum, Norway.

[28] ISO 19902:2020. (2020). Petroleum and natural gas industries-Fixed steel offshore structures. International Organization for Standardization (ISO), Geneva, Switzerland.

[29] Rasul, A., Karuppanan, S., Perumal, V., Ovinis, M., & Iqbal, M. (2024). An artificial neural network model for determining stress concentration factors for fatigue design of tubular T-joint under compressive loads. International Journal of Structural Integrity, 15(4), 633–652. doi:10.1108/IJSI-02-2024-0034.

[30] Ahmadi, H., Lotfollahi-Yaghin, M. A., & Aminfar, M. H. (2011). Geometrical effect on SCF distribution in uni-planar tubular DKT-joints under axial loads. Journal of Constructional Steel Research, 67(8), 1282–1291. doi:10.1016/j.jcsr.2011.03.011.

[31] Lotfollahi-Yaghin, M. A., & Ahmadi, H. (2010). Effect of geometrical parameters on SCF distribution along the weld toe of tubular KT-joints under balanced axial loads. International Journal of Fatigue, 32(4), 703–719. doi:10.1016/j.ijfatigue.2009.10.008.

[32] Chang, E., & Dover, W. D. (1996). Stress concentration factor parametric equations for tubular X and DT joints. International Journal of Fatigue, 18(6), 363–387. doi:10.1016/0142-1123(96)00017-5.

[33] N'Diaye, A., Hariri, S., Pluvinage, G., & Azari, Z. (2009). Stress concentration factor analysis for welded, notched tubular T-joints under combined axial, bending and dynamic loading. International Journal of Fatigue, 31(2), 367–374. doi:10.1016/j.ijfatigue.2008.07.014.

[34] Lo, M., Karuppanan, S., & Ovinis, M. (2022). ANN-and FEA-Based Assessment Equation for a Corroded Pipeline with a Single Corrosion Defect. Journal of Marine Science and Engineering, 10(4), 476. doi:10.3390/jmse10040476.

[35] Miao, K., Pan, Z., Chen, A., Wei, Y., & Zhang, Y. (2023). Machine learning-based model for the ultimate strength of circular concrete-filled fiber-reinforced polymer–steel composite tube columns. Construction and Building Materials, 394(May), 132134. doi:10.1016/j.conbuildmat.2023.132134.

[36] Rasul, A., Karuppanan, S., Perumal, V., Ovinis, M., Iqbal, M., & Alam, K. (2024). Empirical modeling of stress concentration factors using artificial neural networks for fatigue design of tubular T-joint under in-plane and out-of-Plane bending moments. International Journal of Structural Integrity, 15(4), 757–776. doi:10.1108/ijsi-03-2024-0043.

[37] Iqbal, M., Karuppanan, S., Perumal, V., Ovinis, M., & Hina, A. (2023). An Artificial Neural Network Model for the Stress Concentration Factors in KT-Joints Subjected to Axial Compressive Load. Materials Science Forum, 1103, 163–175. doi:10.4028/p-ypo50i.

[38] ANSYS. (2022). Ansys Workbench | Simulation Integration Platform. Ansys, Canonsburg, United States.

[39] MathWorks. (2021). R2021a - Updates to the MATLAB and Simulink product families - MATLAB & Simulink. MathWorks, Natick, United States.

[40] PTC. (2023). Creo CAD Software: Enable the Latest in Design. PTC, Boston, United States.

[41] N'Diaye, A., Hariri, S., Pluvinage, G., & Azari, Z. (2007). Stress concentration factor analysis for notched welded tubular T-joints. International Journal of Fatigue, 29(8), 1554–1570. doi:10.1016/j.ijfatigue.2006.10.030.

[42] Iqbal, M., Karuppanan, S., Perumal, V., Ovinis, M., & Iqbal, M. (2025). Design and Testing of a Test Rig for Tubular Joints Hot-Spot Stress Determination. Results in Engineering, 25(January), 103931. doi:10.1016/j.rineng.2025.103931.

[43] AWS D1.1/D1.1M:2020. (2020). Structural Welding Code-Steel. American National Standards Institute, Washington, United States.

[44] Hectors, K., & De Waele, W. (2021). Influence of weld geometry on stress concentration factor distributions in tubular joints. Journal of Constructional Steel Research, 176. doi:10.1016/j.jcsr.2020.106376.

[45] Paradowska, A., Price, J. W. H., Dayawansa, P., Kerezsi, B., Zhao, X. L., & Ibrahim, R. (2006). Study of influence of post weld heat treatment on residual stress distribution in tubular joints. Welding Research Abroad, 52(2), 10-19.

[46] Masilamani, R., & Nallayarasu, S. (2021). Experimental and numerical investigation of ultimate strength of ring-stiffened tubular T-joints under axial compression. Applied Ocean Research, 109, 102576. doi:10.1016/j.apor.2021.102576.

[47] Iqbal, M., Karuppanan, S., Perumal, V., Ovinis, M., & Khan, A. (2025). Stress Concentration Factors in CFRP-Reinforced KT-Joints under Multiplanar Bending Loads: Experimental and Numerical Investigation. Results in Engineering, 25, 103745. doi:10.1016/j.rineng.2024.103745.

[48] IIW-XV-E. (1999). Recommended fatigue design procedure for welded hollow section joints. International Institute of Welding, Yutz, France.

[49] Koric, S., Viswantah, A., Abueidda, D. W., Sobh, N. A., & Khan, K. (2024). Deep learning operator network for plastic deformation with variable loads and material properties. Engineering with Computers, 40(2), 917–929. doi:10.1007/s00366-023-01822-x.

[50] Kumar, S. D. V., Karuppanan, S., & Ovinis, M. (2021). Failure pressure prediction of high toughness pipeline with a single corrosion defect subjected to combined loadings using artificial neural network (Ann). Metals, 11(2), 1–25. doi:10.3390/met11020373.

[51] Panchal, F. S., & Panchal, M. (2014). Review on methods of selecting number of hidden nodes in artificial neural network. International Journal of Computer Science and Mobile Computing, 3(11), 455-464.

[52] Ahmadi, H., & Lotfollahi-Yaghin, M. A. (2015). Stress concentration due to in-plane bending (IPB) loads in ring-stiffened tubular KT-joints of offshore structures: Parametric study and design formulation. Applied Ocean Research, 51, 54–66. doi:10.1016/j.apor.2015.02.009.